Applied Catalysis B: Environmental 130–131 (2013) 314–324

Contents lists available at SciVerse ScienceDirect

Applied Catalysis B: Environmental

journal homepage: www.elsevier.com/locate/apcatb

Investigation of a molybdenum-containing silica catalyst synthesized by the sol–gel process in heterogeneous catalytic esterification reactions using methanol and ethanol

Alesandro Bail[a], Vannia Cristina dos Santos[a], Marianne Roque de Freitas[a], Luiz Pereira Ramos[b], Wido Herwig Schreiner[c], Gustavo Pimenta Ricci[d], Katia Jorge Ciuffi[d], Shirley Nakagaki[a,*]

[a] Universidade Federal do Paraná (UFPR), Departamento de Química, Laboratório de Química Bioinorgânica e Catálise, CP 19081, CEP 81531-990, Curitiba, Paraná, Brazil
[b] Universidade Federal do Paraná (UFPR), Departamento de Química, Centro de Pesquisas em Química Aplicada – CEPESQ, CP 19081, CEP 81531-990, Curitiba, Paraná, Brazil
[c] Universidade Federal do Paraná (UFPR), Departamento de Física – Laboratório de Sólidos e Interface, CP 19081, CEP 81531-990, Curitiba, Paraná, Brazil
[d] Universidade de Franca, Grupo Sol–Gel, Franca, São Paulo, Brazil

ARTICLE INFO

Article history:
Received 9 April 2012
Received in revised form 1 October 2012
Accepted 9 November 2012
Available online 19 November 2012

Keywords:
Molybdenum
Heterogeneous catalysis
Esterification
Biodiesel
Acid sites
Silica
Sol–gel process

ABSTRACT

Molybdenum-containing silica easily synthesized by the sol–gel process was evaluated as catalyst for heterogeneous esterification reaction of fatty acids using methanol and ethanol. The molybdenum content depended on the conditions employed during the synthesis. The solids were characterized by X-ray powder diffraction, textural analysis, X-ray photoelectronic spectroscopy, and inductively coupled plasma optical emission spectroscopy. The strength and distribution of the acid sites were assessed by the adsorption–desorption of *n*-butylamine as monitored by Fourier transform infrared spectroscopy and thermogravimetric analysis. Kinetic studies revealed high fatty acid conversion for both alcohols and diminished activity upon decreasing concentration of acid sites. Monitoring of the acid sites during the recycling experiments indicated association of the catalytic activity with Mo oxide species on the surface and with the availability of molybdenum-active sites displaying Brønsted–Lowry acidity in the silica structure.

1. Introduction

In the last few years, the demand for sustainability has forced adaptations of well-established industrial processes, so their replacement with green processes is a matter of time. Besides being economically and technically viable, a modern process must enable sustainable development, that is, it must allow for the prosperity of mankind without compromising the potential advancements and quality of life of the future generations [1].

A representative example of sustainable development comes from the energy sector, which has undergone substantial changes due to the increasing participation of renewable energy sources in the energy matrix worldwide. One example is the substitution of petroleum-based diesel for biodiesel, which is a mixture of long-chain alkyl esters obtained from renewable sources, such as vegetable oils and animal fat [2].

Owing to its physicochemical properties, biodiesel is an ideal substitute for fossil diesel that is already being used worldwide. In Brazil, several segments of the society have been involved in biodiesel deployment and utilization. In January 2008, the Brazilian government established the mandatory use of biodiesel blends and determined that all diesel consumed nationwide must contain 2% biodiesel (B2) and reach the B5 level by January 2012. Currently, Brazil is the fourth largest world producer and the third largest world consumer of biodiesel, with an estimated production capacity of nearly 5 million tons per year [3].

The most usual process of biodiesel production consists in the transesterification of vegetable oils and/or the esterification of fatty acids with methanol or ethanol, which is accomplished by homogeneous catalysis. Nevertheless, this process generates a large quantity of waste and consumes raw materials coming from non-renewable sources. In this sense, catalysis has an important role in providing biodiesel production with the expected sustainable character. More specifically, the use of heterogeneous catalysts that can be recovered from the reaction medium and recycled can help minimize the formation of residues [4]. Furthermore, considering that methanol production is mostly based on non-renewable sources, it would be interesting to promote the use of ethanol, in order to obtain a fully renewable fuel [5,6].

Among the various types of catalysts reported in the literature (e.g., oxides, oxosalts, zeolites, layered double hydroxides, ion-exchange resins, and enzymes), the transition metal oxides have

* Corresponding author. Fax: +55 41 33613180.
E-mail address: shirleyn@ufpr.br (S. Nakagaki).

0926-3373/$ – see front matter © 2012 Elsevier B.V. All rights reserved.
http://dx.doi.org/10.1016/j.apcatb.2012.11.009

emerged as an attractive alternative due to their stability, reasonably low cost, easy preparation, and high catalytic activity, the latter of which is mainly related to their Lewis and Brønsted–Lowry acidity [7,8].

In this context, molybdenum-based catalysts, which are applied as acid catalysts in various types of reactions, have also been investigated as catalysts for the esterification/transesterification of fatty acids for biodiesel production [9].

Umbarkar et al. have synthesized mesoporous MoO_3/SiO_2 by the sol–gel process and evaluated it as catalyst for the acetalization of glycerol with various aldehydes [10]. These authors found that the silica with the highest loading investigated in their work (MoO_3/SiO_2 with 20 mol% MoO_3) was the most active catalyst for acetalization under mild conditions. Indeed, maximum conversion of benzaldehyde (72 wt%) was obtained within 8 h at 100 °C, with 60% selectivity for the six-membered acetal.

Recently, the oxosalt anhydrous sodium molybdate has been proposed as an efficient heterogeneous catalyst for the transesterification of the soybean oil. A yield around 96 wt% of methyl esters has been reached under mild experimental conditions [11]. This result and others indicate the potential application of solids containing oxo-metal species as efficient catalysts, because they are considered to be acid sites [8,12].

Catalysts based on Mo/V/W-mixed oxides have been prepared and used in the oxidation of acrolein to acrylic acid [13]. Molybdenum oxides were immobilized on different supports like benzimidazole-functionalized dendrons [14], alumina [15,16], titania [17], zirconia [18], and silica [19,20], for use as catalyst in different process; e.g., catalytic oxidation of ethanol with air, esterification of acetic acid with *n*-butanol and ethanol, transesterification of sunflower oil with methanol, and transesterification of dimethyl oxalate (DMO) with phenol.

A large variety of molybdenum complexes and molybdenum carbonyl compounds have also been immobilized on different inorganic and organic solids such as mesoporous MCM-41and in Mg/Al hydrotalcite (HTC) [21–23]; hybrid matrix synthesized by the sol–gel process, classed as ureasil, which combines a reticulated siliceous backbone linked by short polyether-based segments [24]; crystal-like mesoporous phenylene-silica [25]; polymers (e.g., polybenzimidazole, polystyrene 2-(aminomethyl)pyridine, and poly(4-vinylpyridine) [26,27]); and hydrotalcite clay materials [28]. The resulting solids have been used as catalysts for the oxidation of different substrates, like *cis*-cyclooctene, cyclohexene, styrene, 1-octene, *trans*-2-octene, (*R*)-(+)-limonene, and *R*-pinene.

The use of heterogenized molybdenum and rhenium compounds in different inorganic solids as catalyst for chiral catalytic reactions has been revised recently [29].

The sol–gel process has been widely employed for the immobilization of catalytic species because it allows for the simultaneous control of textural properties and homogeneity [30,31]. The hydrolytic sol–gel route is a two-step process catalyzed in either acidic or basic conditions. It involves a kinetically controlled hydrolytic polycondensation around the silicon atom through substitution of the alkoxide groups via the nucleophilic attack of water molecules, with consequent elimination of the corresponding alcohol [32]. The siloxane (Si–O–Si) group is produced as an intermediate species, which leads to the formation of an amorphous silica framework [33]. Catalytically active compounds may be heterogenized during the silica formation step, which modifies their textural properties and can prompt the generation and optimization of the exposure of the active sites.

In this work, the sol–gel process was used to prepare a molybdenum-containing silica catalyst for the esterification of fatty acids in heterogeneous medium. Among other techniques, the adsorption–desorption of *n*-butylamine was monitored by thermogravimetric analysis, and the concentration of acid sites was determined.

2. Experimental

2.1. Materials

Molybdenum trioxide (MoO_3), tetraethylorthosilicate (TEOS), and lauric acid were purchased from Sigma–Aldrich, Fluka, and Sigma–Aldrich, respectively. Unless specified otherwise, all the other reagents were supplied by Sigma–Aldrich, Acros, or Fluka in analytical grade and used as received; i.e., without further purification.

2.2. Catalysts preparation

The molybdenum-containing precursor was synthesized according to a previously reported method [11]. To this end, MoO_3 (10.0 g) was dissolved in a hot aqueous solution of ammonia 28 wt% (40.0 mL), and a white crystalline powder precipitated after the addition of ethanol (300 mL). The solid was washed in alcohol and dried at 120 °C overnight.

The molybdenum species was immobilized on silica obtained by the sol–gel process. For this purpose, the Mo-containing precursor (stoichiometric excess) was dissolved in 1.10 mol L^{-1} hydrochloric acid solution. The resulting solution was added to the TEOS ethanolic solution (Table 1), and the mixture was stirred for 1 h at 50 °C. Next, the mixture was allowed to stand for 168 h, at this same temperature. The resulting solid catalysts (xerogels) were washed with water and ethanol, treated at 400 °C for 4 h, and labeled as SM1, SM1A, SM2, SM2A and SM3A, depending on the molybdenum content.

2.3. Catalytic experiments

The esterification reactions were performed at the vapor pressure of the alcohol, inside a 15 mL closed teflon cup fitted into a stainless closed vessel reactor. The reactor was maintained at constant temperature and magnetic stirring at 1250 rpm. The fatty acid (1.0 g), an appropriate amount of the alcohol, and the solid catalyst were added to the reaction vessel, and the mixture was stirred vigorously under the vapor pressure of the alcohol for the required reaction time. After cooling to room temperature, the mixture was centrifuged, and the solid catalyst was recovered for reuse. To this end, the catalysts were washed with ethanol (10.0 mL), dried at 120 °C, and their recycling capacity was evaluated in similar sequential reactions. The excess alcohol was removed by evaporation under low pressure, and the conversion of the fatty acid to alkyl esters was assayed by titration of the remaining acidity using a 0.01 mol L^{-1} NaOH standard solution. Experiments were conducted under the same experimental conditions, namely at a catalyst concentration of 10.0 wt% in relation to the acid weight and thermal bath set to 120 °C. The reaction time was adjusted to the kinetics of each fatty acid. A kinetic study was carried out in the range 3–25 h for the lauric acid/alcohol molar ratios of 1:12 and in the range 1–9 h for the oleic acid/ethanol molar ratio of 1:12.

2.4. Recycling experiments

The solid catalyst SM3A was selected for accomplishment of the recycling experiments. For this purpose, SM3A was recovered from the reaction medium by centrifugation and washed with ethanol (15 mL), for removal of the organic phase. This was followed by drying at 120 °C. The resulting recovered catalyst was designated SM3B and was used in a further transesterification reaction. After this first reuse, SM3B was recovered, washed, and dried again, and

Table 1
Conditions used for the preparation of the molybdenum-containing silica solids synthesized by the hydrolytic sol–gel route in acid medium. The results were obtained by ICP-OES analysis.

Sample name	Molar ratio (mol/mol)		Mo added (mmol)[a]	Immobilization tax of Mo after the reaction (%)[b]	Mo content (%)[c]
	H_2O/TEOS	H_2O/H^+			
MoO_3	–	–	–	–	98.3
Precursor	–	–	–	–	76.4
SM1	10	50	0.658	25	0.46
SM1A	10	50	0.963	23	0.62
SM2	10	50	1.38	19	0.72
SM2A	10	50	2.84	16	1.32
SM3A	20	50	5.01	13	1.84

[a] Quantity of molybdenum added to the solid preparation reaction based on the previously determined precursor content.
[b] From the total of Mo added to the reaction; the immobilization percentage rate is the Mo percentage that in fact remained on the prepared solid.
[c] Maximum error in ICP-OES analysis ± 0.85 wt%.

it was then labeled SM3C. The latter solid was employed in a further esterification reaction.

2.5. Characterization techniques

The synthesized silica catalysts obtained by the sol–gel process and the precursors were characterized by X-ray diffraction (XRD), textural analysis, X-ray photoelectronic spectroscopy (XPS), inductively coupled plasma optical emission spectroscopy (ICP-OES), Fourier transform infrared spectroscopy (FTIR), and thermogravimetric analysis (TGA).

For the XRD measurements, self-oriented films were placed on neutral glass sample holders. Measurements were performed in the reflection mode within the range of 3–50° (2θ), using a Shimadzu XRD-6000 diffractometer operating at 40 kV and 30 mA (Cu-Kα radiation λ = 1.5418 Å) with a dwell time of 2°/min.

XPS spectra were recorded on a VG ESCA 3000 instrument with a base pressure of 2×10^{-10} mbar. Mg Kα (1253.6 eV) radiation was employed, and the overall energy resolution of the collected spectra was approximately 0.8 eV. The energy scale was calibrated using the Fermi level and the adventitious C 1s peak at 284 eV. The spectra were normalized to the maximum intensity after subtraction of a constant background.

The specific surface area and the average pore diameter of the catalysts were determined by applying the BET [34] and the BJH [35] methods, respectively, to the corresponding nitrogen adsorption isotherms, which were obtained in a Micrometrics ASAP 2020 physical adsorption analyzer. The samples were previously degassed by treatment at 180–200 °C, until the system pressure reached 10 μmHg. The nitrogen adsorption data were acquired using 0.2 g of the sample.

The Mo content in the catalysts, including monitoring of the recycling reactions, was monitored by ICP-OES on a Thermo Scientific iCAP 6500 spectrometer. A sample of the solid catalyst (15 mg) was submitted to acid digestion under reflux with a mixture of 1.0 mL of 30 vol% hydrofluoric acid and 1.0 mL of 5.0 wt% nitric acid for 1 h, until total dissolution. The solution was filtered through a 0.45-micron membrane and transferred to a 10 mL volumetric flask. An alkyl ester sample (1.0 g) was submitted to strong acid digestion with 1.0 mL of H_2SO_4 98 wt% at 400 °C, for 4 h. The inorganic solid residue was dissolved in HNO_3 5.0 wt% solution, filtered through a 0.45-micron membrane, and transferred to a 10 mL volumetric flask. The concentration of molybdenum was obtained by external calibration.

The strength and distribution of the acid sites on the surface of the Mo-containing silica catalysts were monitored by two different techniques. Before analysis, a sample of the catalyst was treated at 400 °C for 1 h under flowing Ar, in order to activate the surface, and the catalyst was subjected to the *n*-butylamine stream in a glass-degassed vessel kept at 120 °C for 1 h. Then, the catalysts were cooled under flowing Ar, until room temperature was reached. Samples containing *n*-butylamine were characterized by FTIR and TGA. FTIR analysis was accomplished on a Bio-Rad FTS 35000GX spectrophotometer with KBr discs prepared after mixing (1 wt%) each of the test samples with anhydrous KBr. Experiments were performed in the transmission mode in the 400–4000 cm^{-1} range, with a resolution of 2 cm^{-1} and accumulation of 16 scans. TGA analysis was simultaneously conducted on a Thermal Analyst 2100 from TA Instruments SDT Q600 with simultaneous DTA–TG. The analyses were undertaken in nitrogen atmosphere, at a heating rate of 20 °C/min, from 25 to 1000 °C.

3. Results and discussion

3.1. Preparation of the catalysts

The molybdenum-containing precursor was previously synthesized by dissolution of MoO_3 in highly alkaline medium. As a result, a white-crystalline solid with structure derived from the ammonium paramolybdate was formed (as discussed further ahead). This synthetic approach was important because it avoided the presence of stable Na^+ and K^+ ions that usually remain in the material even after thermal treatment at high temperatures (i.e., above 400 °C). The presence of the latter ions is undesirable, because their strongly basic character favors their stabilization in the oxide phase, culminating in a parallel activity [36] that compromises the investigation of the catalytic activity of Mo-systems. A further advantage of this synthetic approach is that the NH_4^+ ions can be replaced with H^+ ions coming from the superficial water after the thermal treatment, thereby giving rise to Brønsted–Lowry acid sites on the surface of the solid.

The sol–gel process was employed for the preparation of the silica catalysts containing immobilized molybdenum, aiming at a homogeneous distribution of the molybdenum sites on the surface of the solid. Another reason for utilizing this process was that the hydrolytic sol–gel route can improve the interaction between the molybdenum sites and the silica matrix during the hydrolysis and condensation steps, thereby minimizing further Mo losses by leaching or inactivation. Both the acid and the basic hydrolytic sol–gel routes were tested, but only the catalysts achieved via the acid route furnished materials with detectable levels of Mo on their surface, possibly because of the intermediate species generated during the TEOS hydrolysis step. During this step there is protonation of the alkoxide group, which is followed by a nucleophilic attack of the water molecule, with consequent formation of a pentacoordinate intermediate. Electronic density is therefore withdrawn from the silicon atom, making it more electrophilic and more susceptible to attack from water and enhancing the

leaving group character of the alkoxide [33]. Hence, the polyanion derived from the molybdate structure, typically produced under controlled acidic conditions [37], may have interfered in the mechanism by destabilizing the positive intermediate and producing molybdenum-containing siloxane species such as Si–O–Mo–O–Si. On the other hand, the polyanions may have acquired an inert behavior during the TEOS hydrolysis and condensation steps when they became trapped inside the silica. Table 1 summarizes the major experimental parameters used in the synthesis of the silica catalysts investigated in this work, as well as the molybdenum content obtained by ICP-OES analysis and their immobilization rate. The solid catalysts were labeled as SM1, SM1A, SM2, SM2A, and SM3A, depending on their molybdenum content. During the catalytic recycling experiments, the solid SM3A recovered after the first use was renamed SM3B and reused as catalyst (second use). The same was done for SM3B recovered after the second use, which was relabeled SM3B and reutilized as catalyst, too (third use).

Increasing the amount of molybdenum that was added during the synthesis favored larger molybdenum content in the catalysts. The catalyst SM1 had the lowest Mo content (0.42 wt%), whereas the catalyst SM3A displayed the highest Mo content, 1.84 wt%. This trend is certainly linked to the availability of Mo ionic species during the steps of hydrolysis and condensation of the silica network. Moreover, the rise in the Mo content was not proportional to the increase in the mass of precursor utilized in the reaction, indicating that the immobilization rate dropped with higher molybdenum quantities. Therefore, the immobilization of Mo species should reach a maximum level that would depend on the capacity of the silica network to incorporate this metal, which agrees with the Fick's laws of diffusion in solids [38]. Furthermore, the elevation in the H_2O/TEOS molar ratio may have contributed to the diminished immobilization of Mo species. This might have been due to the dilution factor, which hinders the contact between the reactant species [39]. The Mo-containing precursor exhibited a Mo content of 76.4 wt%, which was higher than the Mo content expected for compounds such as ammonium molybdate (49 wt%) and ammonium paramolybdate (57 wt%). In summary, the conditions employed during the synthesis promoted the formation of a solid precursor with a complex structure that displayed a high Mo content.

The XRD patterns of the catalysts studied in this work as well as the precursors are shown in Fig. 1. The Mo-containing precursor (Fig. 1c) presented the main diffraction peaks at $2\theta = 14.020$ and 26.722. The crystalline structure of the precursor was thus similar to that of ammonium paramolybdate [40], with a high proportion of Mo atoms. MoO_3 (Fig. 1a) displayed an XRD profile with different diffraction peaks; namely at $2\theta = 12.868$, 23.408, 25.788, 27.408, and 39.068, which correspond to the 0 0 1, 1 0 1, 0 0 2, 0 1 1, and 1 0 2 diffraction planes, respectively, typical of the MoO_3 monoclinic crystalline system. The silica synthesized by sol–gel process in the absence of molybdenum compounds (control solid) exhibited a halo characteristic of amorphous silica, with a maximum located between $2\theta = 15$ and 30° (Fig. 1b). The catalysts SM1 and SM2 (low Mo content) did not have any detectable diffraction peaks. There was only an amorphous halo, which can be assigned to the high dispersion of the immobilized Mo species (Fig. 1d and e). Despite the low intensity, the catalyst SM3A displayed some peaks that are quite similar to those achieved for MoO_3 (Fig. 1f). This suggests that the high Mo content and the thermal treatment at 400 °C may have favored the formation of MoO_3 crystals over the surface of the silica [41–44].

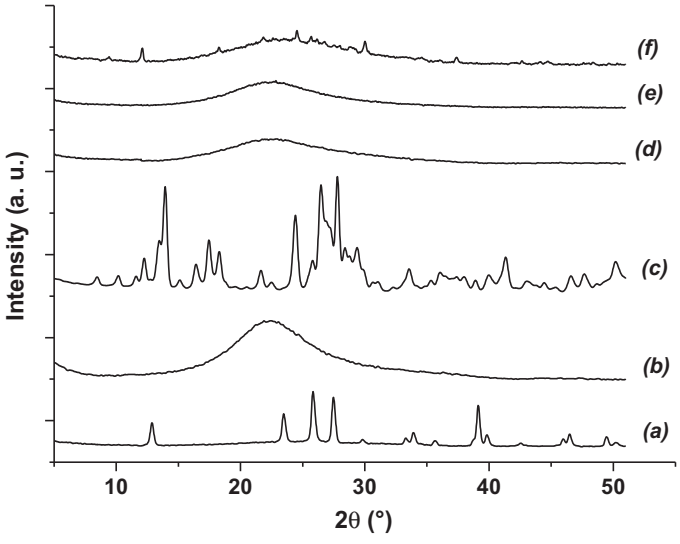

Fig. 1. XRD analyses of the solids: (a) MoO_3, (b) silica solid – control, (c) precursor, (d) SM1, (e) SM2, and (f) SM3A.

Table 2
Physical properties deduced from N_2 adsorption onto the silica solids prepared by the sol–gel process at 77 K.

Sample	Specific surface area ($m^2\ g^{-1}$)	Average pore size (nm)	Pore volume ($cm^3\ g^{-1}$)
SM1	434	5.7	0.62
SM2	410	6.0	0.62
SM3A	14	13.3	0.045

Fig. 2a–c depicts the XPS spectra recorded for the synthesized catalysts in the Mo 3d region. After mathematical treatment for deconvolution of the spectra, we observed two peaks related to the binding energy of the Mo $3d_{5/2}$ and $3d_{3/2}$ orbitals, at approximately 232.7 and 235.7 eV, respectively. According to Plyuto et al., the definition of the spectra can be compromised by the low concentration of MoO_3 in the samples, but it is still possible to realize that the results agree with those reported earlier for the supported molybdenum oxo-species in the highest oxidation state [45]. Indeed, the intensity of the signal augmented on going from SM1 (Fig. 2a) to SM3A (Fig. 2c). Typically, the binding energy of MoO_3 appears at 231.7 eV ($3d_{5/2}$), a region with energy lower than 232.7 eV [46]. The shift to a higher energy region in relation to the pattern of MoO_3 that was detected in the spectra of all the synthesized catalysts is due to the strong interactions taking place between the oxo-molybdenum species and the hydroxyl groups of the silica support.

The oxidation state of the immobilized metal oxide is extremely important for this class of catalysts. According to Fig. 2a–c, the presence of molybdenum(VI), i.e., the metal in its highest oxidation state, may account for the Lewis acidity of these catalysts, which is related to the high metal load/metal radius ratio and the stabilization of pairs of electrons coming from π-donor species, such as the carboxyl and carbonyl groups present in the triacylglycerol and fatty acid molecules, or an alcohol molecule acting as a nucleophile [47].

Table 2 presents the different textural characteristics of the synthesized systems. The catalysts SM1 and SM2, which showed the lowest Mo content, have higher specific surface area, approximately 30 times higher than that of the catalyst SM3A. The catalyst SM3A displayed an average pore diameter around 13.3 nm, greater than the average pore diameter of the other catalysts SM1 and SM2, around 6.0 nm.

The solid catalysts had varied pore size distribution (Fig. 2d–f), including large diameter pore in the case of SM3A, around 60 nm, which features a macroporous solid [48]. These results agree with the adsorption isotherms (Fig. 2g–i) of the catalysts, since samples SM1 and SM2 presented Type-IV isotherms, which are characteristic of mesoporous materials, while the isotherm of sample SM3A

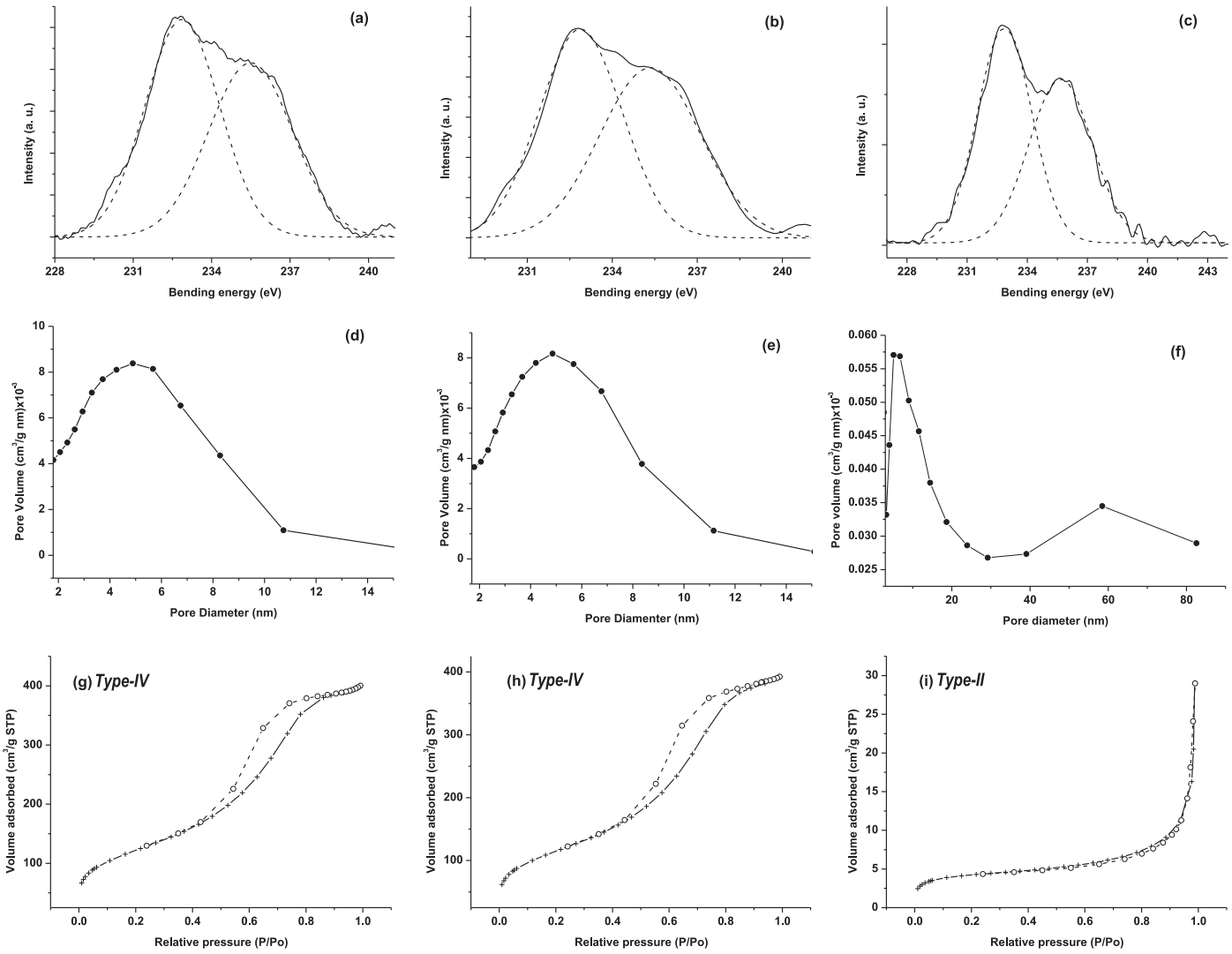

Fig. 2. XPS spectra of the Mo 3d region for (a) SM1, (b) SM2, and (c) SM3A. The continuous line corresponds to the experimental results, while the dashed line is the result of the deconvolution treatment of the experimental data. Pore size distribution of the solids (d) SM1, (e) SM2 and (f) SM3A, synthesized by the sol–gel process. Nitrogen physisorption isotherms at 77 K for the synthesized catalysts: (+) adsorption, (○) desorption. (g) SM1, (h) SM2 and (i) SM3A.

was Type-II, typical of macroporous materials (Type-II isotherms can also be related to nonporous materials, but the pore size distribution of the sample SM3A, Fig. 2f, shows that this is not the case here). In addition, the isotherm of the sample SM3A did not reveal hysteresis, which is typical of solids with high pore size dispersion. The isotherms of samples SM1 and SM2 samples exhibited H1 hysteresis loops, which is evidence of ordered porosity, with the pores having uniform shape and size (in the case of size, this hypothesis can be confirmed by the respective pore size distributions, Fig. 2d and f) [48].

Thus, it seems that the high H_2O/TEOS molar ratio used in the experiments (Table 1) enabled the formation of solids with high specific surface area and small pore size (mesopores) [49]. However, the high concentration of Mo-containing ions may have hindered the nucleation step (hydrolysis) during the synthesis of SM3A, facilitating partial packing of the particles. This could lead to formation of blind cylindrical, cone-shaped, or wedge-shaped pores (evidenced by the absence of hysteresis), which are larger than the mesopores of samples SM1 and SM2, culminating in decreased surface area. Furthermore, the reduction in both surface area and pore volume can also be explained by MoO_3 crystal formation over the silica surface (already discussed on the basis of XRD, Fig. 1c). Smaller surface area upon increased doping with the metallic ion is frequently observed in the literature [48,50].

3.2. Catalytic activity

3.2.1. Investigation of the distribution and strength of the acid sites

The distribution and strength of the acid sites in the synthesized catalysts were evaluated by using *n*-butylamine as probe. This molecule adsorbs onto different types of sites, with distinct intensity. FTIR was employed for the qualitative monitoring of the existence of acid sites on the basis of the vibrational modes of the probe molecule (Fig. 3). The peaks at 1200, 1100, and 800 cm^{-1} are characteristic of the SiO_2 solid and were attributed to the Si–O stretching vibration, while the band at 470 cm^{-1} was ascribed to Si–O angular deformation. The band at 974 cm^{-1} was assigned to the stretching vibration of the silanol group. In the spectrum of the synthesized catalyst, the bands at 1100 and 974 cm^{-1} were slightly shifted in relation to the vibrations of the Si–O and SiOH groups, respectively. This may indicate interaction of Mo-species in the structure of the silica, due to the binary oxide generated during the sol–gel process and subsequent heat-treatment [51]. IR patterns corresponding to the control (silica in the absence of

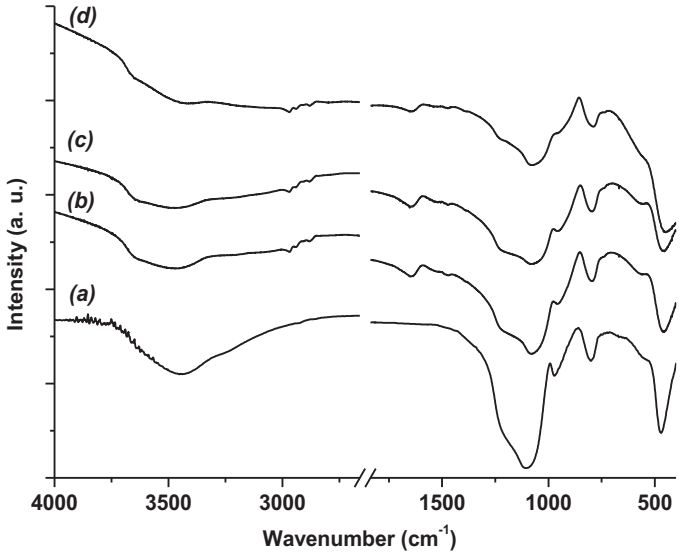

Fig. 3. FTIR spectra of the solids submitted to *n*-butylamine adsorption under controlled conditions: (a) silica, (b) SM1, (c) SM2, and (d) SM3A.

Mo-species) did not evidence any peaks related to the adsorption of *n*-butylamine in the 1300–1700 cm^{-1} range (Fig. 3a). The profiles of the remaining catalysts were similar, with a peak at 1645 cm^{-1}, attributed to the Lewis acid sites, and another at 1475 cm^{-1}, ascribed to the Brønsted–Lowry sites. Some peaks were also detected in the region of 2900 cm^{-1} and were assigned to the CH stretching vibration modes of the *n*-butylamine carbon chain.

The samples containing the probe molecule were submitted to TGA analysis, in order to examine the weight loss profile as a function of the heating rate. Melo et al. observed that the clay mineral paligorskyte submitted to cationic exchange with lanthanum (III) and exposed to atmosphere saturated with *n*-butylamine presented weight loss at different temperatures upon heating up to 800 °C. This indicated that the probe molecule was bound to the sites in different ways, consequently resulting in various levels of acid sites strength and concentration [52,53].

From the weight loss data we estimated the total acidity of the catalysts, since *n*-butylamine (73.14 g mol^{-1}) must be adsorbed onto their active sites. The acidity was calculated for the entire region depicted in Fig. 4, which shows that the silica presented only weak acid sites between 50 and 280 °C, corresponding to the weak Brønsted–Lowry acid sites (Fig. 4a). All the solid catalysts displayed

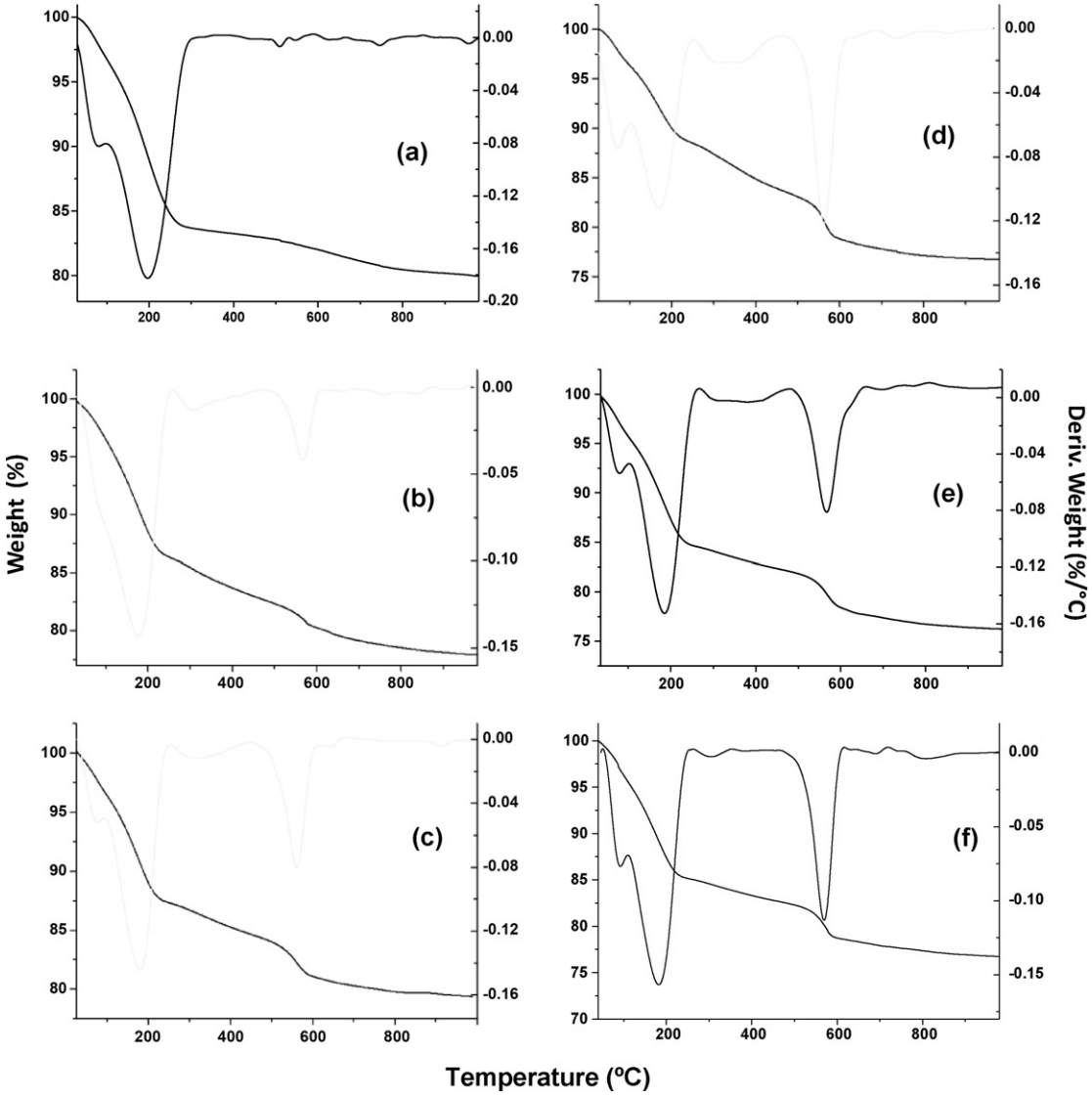

Fig. 4. Thermogravimetric and DTA curves of the samples adsorbed with *n*-butylamine: (a) silica, (b) SM1, (c) SM2, (d) SM3A, (e) SM3B, and (f) SM3C.

Table 3
Acid sites distribution per stage of thermodesorption for the as-synthesized solid catalysts.

Type of adsorption site	SiO_2	SM1	SM2	SM3A	SM3B[a]	SM3C[b]
	(mmol of acid sites/g of solid)					
Physisorption	0.63	1.83[c]	0.514	0.547	0.790	0.783
Weak chemisorption	2.10		1.20	1.02	1.33	1.38
Medium chemisorption	–	0.554	0.404	0.715	0.340	0.355
Strong chemisorption	–	0.388	0.551	0.708	0.665	0.582
Total	2.73	2.76	2.67	2.99	3.12	3.10

[a] First and [b] second recycling. [c] Arbitrarily assigned from TGA analysis: physisorption more weak chemisorptions.

a similar profile in terms of thermal events, classified as desorption of (a) *n*-butylamine molecules physically adsorbed by weak forces (below 110 °C), (b) *n*-butylamine molecules chemisorbed on weak sites (110–230 °C), (c) *n*-butylamine molecules chemisorbed on sites of medium strength (230–480 °C), and (d) *n*-butylamine molecules chemisorbed on strong sites (480–650 °C). There was a small overlap of events for the solid catalyst SM1 (Fig. 4b) in the region from 50 to 230 °C. All the DTA curves exhibited low definition in the region attributed to the acid sites of medium strength. Nevertheless, the profile of acid sites distribution was maintained during the recycling process.

Table 3 brings the general distribution of the acid sites in the synthesized catalysts. The total concentration of acid sites in the solid catalysts was virtually constant. SM1 (low Mo content) and SM3A (high Mo content) had the lowest and highest concentrations of acid sites, respectively. In other words, the concentration of strong acid sites increased with rising Mo content, but interestingly it decreased during the recycling process, indicating partial inactivation or leaching of the metal. For all the solid catalysts SM1, the physical adsorption and weak chemical adsorption sites were not satisfactorily separated into different regions. Therefore, they were considered as a sole desorption event.

According to Fig. 4 and Table 3, the high concentration of acid sites in the synthesized catalysts is proof that the immobilization of Mo species elicited modifications on the surface of the support. As illustrated in Fig. 1, SM3 displayed a set of diffraction peaks and its profile was very similar to that of MoO_3. Owing to the low dispersion of crystals on the surface of the silica, microregions where the Mo species are a major component in relation to SiO_2 may have been created. The reason for the formation of a molybdenum oxide phase on the silica may be twofold. Firstly, the sol–gel process was carried out in acid medium, which may have led to the production of molybdic acid, the hydrated form of molybdenum oxide ($MoO_3{\cdot}2H_2O$). Secondly, heat-treatment at 400 °C might have caused dehydration of the catalyst and consequent formation of MoO_3 on the SiO_2 surface, i.e., a binary oxide was generated. The formation of binary oxides can create an imbalance of charges upon combination of oxides with different oxidation numbers. This culminates in the appearance of both Lewis and Brønsted–Lowry acid sites, characterized by a positive and negative charge residue, respectively. Thus, metal oxides that are normally inactive or slightly active can exhibit high catalytic activity upon combination with other oxides.

Tanabe postulates that the acidity of solids formed from the combination of oxides can be used to predict the acidity of a given mixture of oxides according to the following assumptions: (i) the coordination number of the positive elements is maintained even after the mixture is obtained and (ii) the coordination number of the negative element (oxygen) in the major oxide is preserved for all the oxygen atoms of the binary oxide [54].

According to Smith and Rohrer, some transition metal oxides such as MoO_3 crystallize with distortions, resulting in layered structures [55]. The stereochemistry of the metal atom in MoO_3 can be considered as a distorted octahedral or deduced from the tetrahedral form of MoO_3 as a basic unity. Considering the first assumption, each layer consists of octahedral groups MoO_6 on two levels, which the oxygen atoms assume different coordination numbers ranging from 1 to 3 (Supplementary data, Fig. S1). Furthermore, a schematic representation according to Tanabe postulates that the coordination number of the positive elements in the binary oxide remains 6 and 4 for molybdenum and silicon, respectively [54] (Supplementary data, Fig. S2). In Fig. S2, the excess positive charge evidences the appearance of Lewis acid sites in the case of the structural mode only. The latter represents the situation in which the MoO_3 microcrystals are located in a microregion where MoO_3 is the major component.

Even though Tanabe's postulate helps explain the formation of acid sites in the synthesized catalysts, the results presented in Table 3 point to a very high concentration of acid sites in relation to the Mo concentration in the solids. This evidences that the acid surface of the silica matrix underwent some type of modification, which resulted in increased concentration and strength of the acid sites.

The acidity of solids such as aluminosilicates can be improved by substitution of ions when NH_4^+ instead of Na^+ ions are present in the aqueous solution. After thermal treatment, NH_4^+ can decompose, affording Brønsted–Lowry acid sites due to the presence of an H^+ ion. The formation of such acid sites would not be expected for the catalysts prepared in this work, because the existence of Mo(VI) species leads to a positive residual charge on the structure. However, the high dispersion of pore size in the solids, the types of adsorption isotherms, the heterogeneity and complexity of the particles, and the results obtained by XRD (indicating formation of a crystalline phase in the solid SM3A) and XPS (indicating the presence of Mo in a high oxidation state), it seems more reasonable to attribute the high concentration of acid sites to the formation of a multilayer for adsorption of amine molecules within the complex network of pores. This should make their desorption harder, resulting in very high concentrations of acid sites (Table 3).

3.2.2. Catalytic activity evaluation

We evaluated the catalytic activity of these solids in the heterogeneous catalytic esterification of lauric and oleic acids using methanol and ethanol (Table 4). Interestingly, the different catalysts displayed quite similar activity, regardless of the employed alcohol. This is a favorable feature, because the use of ethanol allows for the attainment of a fully renewable product. Table 4 lists the results of the experiments accomplished using the catalysts SM1, SM1A, SM2 and SM2A, as well as data from the recycling experiments employing SM3A. The solids SM1A and SM2A were prepared and used in order to verify whether solids with much lower molybdenum content than samples SM1 and SM2 would also be active in catalysis.

The results obtained for the reaction conducted in the presence of the silica matrix containing no Mo-species (control solid) and for the esterification reaction of lauric acid in the presence of ethanol only are also shown for comparison purposes. Data from the reaction between oleic acid and ethanol are also presented, since the highest values of conversion and turnover number (TON) were achieved in this case.

As expected (Table 4), the activity of the catalysts depended on the concentration of acid sites for all the solid catalysts, including SM1A and SM2A. The solid SM3A furnished the best result, yielding 95.6 and 97.1 wt% alkyl esters in the presence of ethanol and methanol, respectively (Table 4, reaction 3). The high catalytic activity observed for both alcohols indicates that the experimental conditions were sufficiently drastic, and that the size of the

Table 4
Conversion results for the heterogeneous catalytic esterification reaction of lauric acid catalyzed by Mo-containing silica catalysts.

Reaction	Sample	Conversion into alkyl esters (%)			
		Methanol	TON	Ethanol	TON
1	SM1	55.5 ± 4.7	578	67.2 ± 4.4	700
	SM1A	–	–	71.6 ± 3.2	553
2	SM2	63.7 ± 2.6	424	74.3 ± 2.7	494
	SM2A	–	–	88.4 ± 3.2	320
3	SM3A	97.1 ± 0.85	253	95. 6 ± 2.1	249
4	SM3B	92.0 ± 2.3	266	90.2 ± 2.1	261
5	SM3C	87.1 ± 1.4	280	86.4 ± 4.8	277
6	SM3A (oleic acid)	–	–	95.1 ± 2.0	176
7	Silica (control solid)	11.4 ± 2.7	–	13.8 ± 4.5	–
8	No solid added	<5	–	<5	–

Experimental conditions: lauric acid/alcohol molar ratio 1:12, 10 wt% of catalyst in relation to the acid mass, temperature = 120 °C and reaction time = 15 h. Reaction 6: oleic acid in similar conditions, except for the reaction time, which was 6 h. TON = mol of substrate converted by mol of molybdenum added as active species.

carbon chain of the reaction substrate did not have any significant influence on the catalytic results.

Because silica containing no Mo species (silica control solid) has low or moderate Brønsted–Lowry acidity, the results did not exceed the catalytic conversion of 14 wt% alkyl esters (Table 4, reaction 7). Under solvothermal conditions, in the absence of the catalyst, the conversions were negligible, less than 5 wt% (Table 4, reaction 8).

The dependence of product formation on the concentration of Mo species is clear from results presented in Table 4 are considered. However, in the case of solid catalysts obtained by dispersion of an active phase in an inert matrix, it is necessary to check the degree of commitment of the catalytic system with the phenomenon of resistance to mass transfer on the surface of the solid catalyst. The test proposed by Madon and Boudart, a variable of the method proposed by Korus and Novak, suggests that a catalytic system composed by solid catalysts synthesized under the same experimental conditions and having different concentrations of active species, but containing the same degree of dispersion on the matrix surface, should be evaluated [56,57].

To meet the requirements of the method proposed by Madon and Boudart, we prepared three new solid catalysts under the same experimental conditions as those employed in the synthesis of the catalysts presented in Table 1, except for the amount of Mo that was added to the reaction medium. The new solid catalysts were named SM4, SM5, and SM6, and the Mo concentration considering immobilization of 25 wt% was 46.3, 24.0, and 6.12 μmol Mo/g of solid catalyst, respectively. In this method, the slope of the plot of turnover frequency (TOF) versus the quantity of active sites available for the reaction may be associated with the presence of resistance to mass transfer in the solid catalysts. If the resulting slope is equal to 1, there is no resistance to mass transfer and, presumably, the larger the amount of Mo present in the matrix, the higher the TOF, i.e., the greater the number of mol of converted substrate in relation to a given number of mol of active species [58]. If the slope is close to 0.5, the system experiences resistance to mass transfer inside the particles. The impact of such resistance is not so strong, so even increasing concentrations of Mo in the catalyst promote enhanced activity. If the curve obtained for the correlation between the activity and the availability of Mo has slope equal to zero, there is resistance to mass transfer between the phases in the environment surrounding the particles.

The results from the esterification of oleic acid with ethanol in the presence of SM4, SM5, and SM6 at 120 °C are illustrated in Fig. 5a.

In fact, the catalytic activity of SM4, SM5, and SM6, expressed as turnover frequency (TOF), clearly correlated with the concentration of Mo in the silica matrix. More specifically, the TOF rose with increasing concentration of Mo, but this elevation was not linear. According to the method of Madon and Boudart, mass transfer within the evaluated solid catalysts should be difficult (slope close to 0.5). Fig. 5a shows that the average slope was 0.49, indicating that the MoO_3 deposited on the surface of the matrix probably hindered the access of the substrates to the active sites of Mo located inside the pores. Moreover, according to Table 2, the pore diameter and the surface area of the catalysts SM1, SM2, and SM3, which were used in the catalytic experiments, diminished with increasing Mo concentration. Consequently, the pore volume augmented, suggesting possible filling of the pores of the catalyst with Mo species.

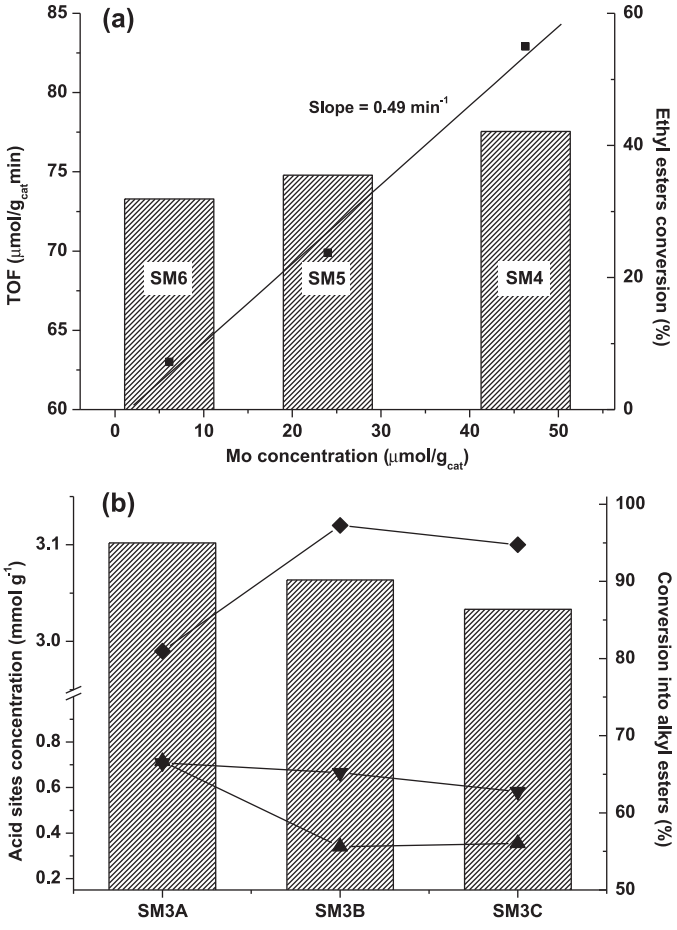

Fig. 5. (a) TOF dependence on the Mo-species concentration in the oleic acid esterification with ethanol at 120 °C. TOF was calculated from the maximum reaction rate (maximum slope) at 3 h. Bars indicate the conversion results as ethyl oleate. (b) Dependence of the concentration of acid sites and conversion into ethyl esters during the recycling experiments. (♦) Total sorption, (▲) medium and (▼) strong chemisorptions.

Therefore, only the species that settled near the upper end of the pores would be accessible to the substrate molecules, and the access to the species that settled at the bottom of the pores would be blocked, as schematically represented in Supplementary data Fig. S3.

Although the results of the first and second reuse were satisfactory (Table 4, reactions 4 and 5), there was a slight decrease in conversion. However, conversion remained practically constant during the recycling experiments if the calculated standard deviation is considered. This apparently reduced catalytic conversion may be associated with the lower concentration of acid sites. In fact, according to Table 4, the concentration of acid sites for medium and strong chemisorption dropped during the recyclability study involving SM3.

ICP-OES analysis of the synthesized alkyl esters indicated Mo content below the limit of detection of the method ($1.0\ \mu g\ L^{-1}$). This evidences that Mo is absent from the reaction solution and suggests that the small portion of molybdenum that possibly leached from the solid catalyst during the catalytic reaction did not remain in the organic phase.

Fig. 5b depicts the dependence of substrate conversion on the concentration of acid sites present in the catalysts SM3A, SM3B, and SM3C during the recycling process. The physisorption and weak chemisorption sites exist in the silica containing no Mo-species, so these sites cannot be associated with the catalytic activity of the studied materials. As for the strong and medium chemisorption acid sites, which are not usual in silica, the reduction in their concentration seems to have accompanied the decrease in the concentration of Mo in the solids. However, according to the information in Table 4, a direct correlation between the strength of a particular acid site and its type, i.e., Lewis or Brønsted–Lowry, cannot be inferred.

According to the results obtained here, it is reasonable to suggest that the catalytic activity of these solids should not be associated with the Lewis and Brønsted–Lowry acid sites related to the immobilized crystalline MoO_3 only. The catalytic activity should also be correlated to the availability of active sites comprised by Mo atoms that are part of the silica network and are more resistant to the leaching process. In line with this assumption, the ICP-OES analysis of the catalysts SM3A, SM3B, and SM3C during the recycling process indicated that the average leaching was approximately 10 wt% after reactions 4 and 5 (Table 4), a value that is close to the reduction in the concentration of strong acid sites during the recycling process. The decrease in the concentration of medium acid sites was not compatible with the concentration of Mo in the catalysts, suggesting that the sites of medium strength are very sensitive. In this sense, considering the complexity of the net of pores formed in the solid SM3, the sites of medium strength may be the most affected by irreversible chemisorption of reactant molecules in a process of deactivation by chemical poisoning. Thus, unlike the Lewis sites, the Brønsted–Lowry acid sites that eventually underwent deactivation could be regenerated, since their concentration in the silica matrix should be approximately constant.

Similar systems have been characterized by a large number of techniques, and it has been demonstrated that there is strong interaction between the metal oxide surface and the inert matrix. It has been proposed that WO_X species exist as isolated tetrahedra connected to the WO_4 support in the system WO_3/Al_2O_3, and that there are two oxygen atoms double bound to each tungsten atom [59]. The Brønsted–Lowry acidity increases due to changes in the configuration of the WO_4 tetrahedron upon alteration of the number of substituent groups around the tungsten atom. In addition, literature reports have described other systems, and we suggest the same kind of chemical environment for Mo immobilized on silica. However, it seems reasonable to expect that the arrangement of the Mo atoms in the systems examined herein results in acid sites that do not have a single identity.

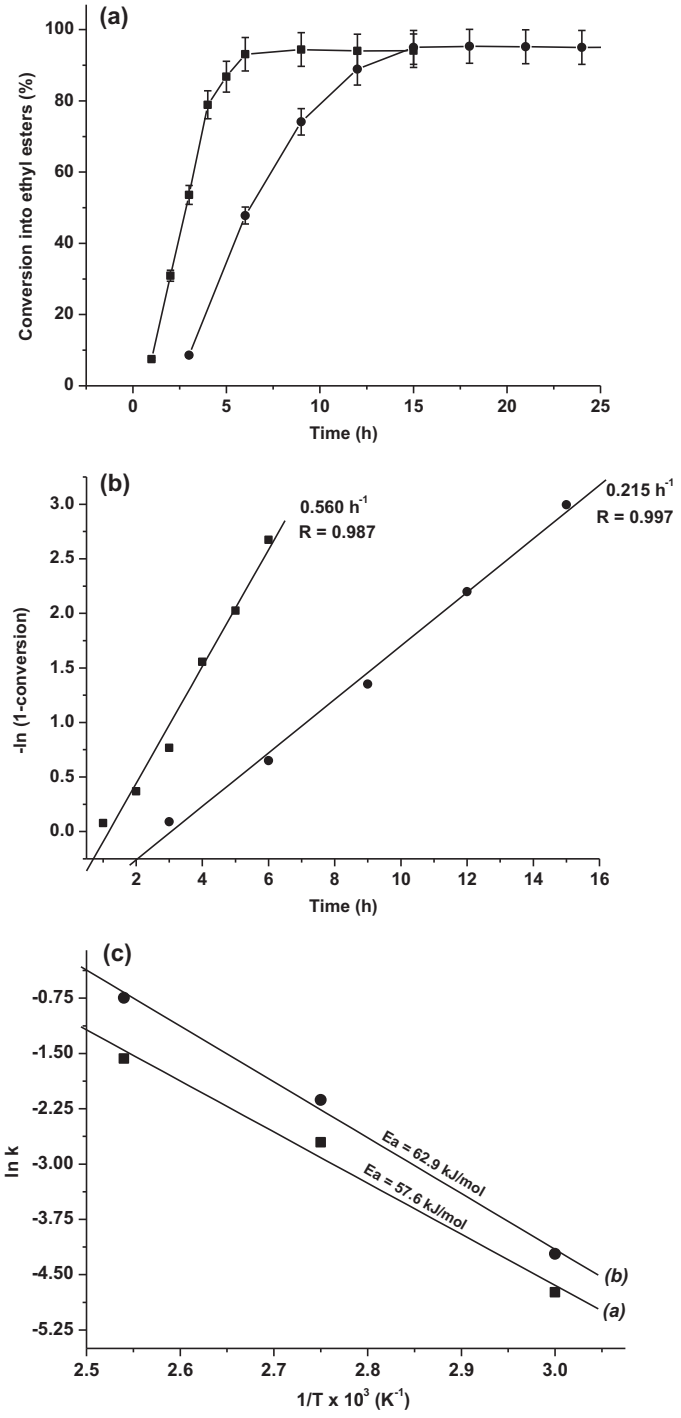

Fig. 6. (a) Kinetics of esterification at different fatty acid/alcohol molar ratios. Maximum error ± 5 wt%, (b) fits assuming pseudo first-order kinetics: (■) 1:12 oleic acid/ethanol and (●)1:12 lauric acid/ethanol and (c) plot of $\ln k$ vs. $1/T$. The slope indicates the activation energy of the esterification of (a) lauric acid and (b) oleic acid with ethanol in the presence of the catalyst SM3A.

3.2.3. Kinetic evaluation

We conducted a study about the dependence of the catalytic conversion results on the reaction time and on the fatty acid/ethanol molar ratio. Fig. 6 presents the kinetics of lauric acid and oleic acid esterification with ethanol at a molar ratio 1:12, catalyzed by SM3A.

Fig. 6a reveals that the lauric acid/ethanol molar ratio of 1:12 afforded the maximum conversion after 15 h. The kinetics of the esterification of oleic acid with ethanol exhibited the same profile,

that is, conversion enhanced as the reaction time increased. However, the maximum conversion (95.1 wt%) was only reached at 6 h of reaction. According to Fig. 6b, the rate constant determined for the esterification of oleic acid ($0.560\ h^{-1}$) is about three times larger than the one achieved for lauric acid ($0.215\ h^{-1}$) in the presence of ethanol and the catalyst SM3A. In other words, under these conditions the esterification of oleic acid is faster than that of lauric acid. This observation suggests that the presence of an unsaturated bond between carbons 9 and 10 of the fatty acid molecule facilitated interaction of oleic acid with the polar surface of the solid catalyst, accelerating the catalytic reaction. Alonso et al. have performed a systematic study of the influence of the polarity of some molecules on the catalysis of transesterification in the presence of catalysts in homogeneous and heterogeneous media [60].

The addition of polar groups (such as bromine) to the molecule of the ester reagent facilitated interaction of molecules with the catalyst surface containing the sulfonate group. Thus, the unsaturated oleic acid elicited an increase in the polarity of the fatty acid molecule that was large enough to facilitate the interaction with the acid sites of the silica surface. Considering that lauric acid is consumed as the alkyl esters are produced, the plot of −ln(1-conversion) versus time provides the reaction order. Fig. 6b represents the possible fits of the esterification reaction of the fatty acid assuming pseudo first-order kinetics. The fitting reveals a linear correlation between the experimental data, which is typical for this type of reaction where the concentration of the alcohol is kept constant. The rate constants k and their corresponding correlation coefficient are displayed along the curves in Fig. 6b.

The reaction activation energy can be calculated by the Arrhenius equation when the reaction rate constants, k, are determined at different temperatures, as follows:

$$k = Ae^{-Ea/RT},$$

where A is the pre-exponential factor, Ea is the activation energy, R is the ideal gas constant, and T is the reaction temperature (K).

Fig. 6c evidences the good linear correlation between $\ln k$ and $1/T$ over the temperature range 60–120 °C.

The activation energy values for the production of ethyl laurate and ethyl oleate, Ea, were 57.6 and 62.9 kJ mol^{-1}, respectively, agreeing with literature reports on myristic acid esterification (22.51 kJ mol^{-1}) [61].

Finally, the catalytic activity of these solids appears to be susceptible to modulation by control of the degree of the MoO_3 phase dispersion, which is deeply associated with the porosity of the solids [62–64]. Compared to other systems and solid acids used in the production of biodiesel, the catalysts presented here have major advantages. More specifically, the sequence of synthetic steps is simplified, allowing for the synthesis of high-purity esters without expensive purification steps.

4. Conclusions

The sol–gel process allowed for the synthesis of Mo-containing silica catalysts with high concentration of acid sites and pronounced catalytic activity for the esterification of fatty acids with methanol or ethanol. Because we prepared a solid material based on catalytic species immobilized on silica obtained by the sol–gel process [10], the catalysts discussed here presented catalytic activity that was directly proportional to the Mo concentration. The solid catalysts were highly resistant in terms of leaching and reuse capacity. In addition, it was possible to recover and recycle the prepared solids. Conversion results near 95% were achieved. Attention to the surface area revealed that the solid SM3A, with very low surface area ($14\ m^2\ g^{-1}$), afforded good catalytic results.

The Tanabe postulate helped us predict the acidity of the resulting binary oxide system. A positive charge residue in the microregions where MoO_3 was the major component confirmed the formation of Lewis acid sites. Moreover, the high acidity of the solids was explained by the appearance of Brønsted–Lowry acid sites due to the different disposition of the oxygen atoms in the MoO_3 structure, which resulted in different coordination numbers. The activity seemed to be related to the Mo content, however, a blocking effect may have occurred in the catalyst SM3A, which might have been caused by Mo-species settled in the top of the pores. A Madon–Boudart test showed that intra-particle mass transfer resistance phenomena influenced the catalytic activity, and this effect became more noticeable as the concentration of Mo-species on the surface of the solid augmented. During the recycling experiments, the conversion decreased. This fact could be related to a reduction in the concentration of acid sites, which was attributed to leaching or inactivation and indicated that these sites are sensitive to the recovery procedures. The good fitting of the experimental results revealed the existence of pseudo first-order dependence in the esterification reactions. We calculated the activation energy for the esterification reactions, and the values were consistent with those expected for this class of reactions.

Acknowledgments

The authors acknowledge the financial support obtained from CAPES (Coordenação de Aperfeiçoamento de Pessoal de Nível Superior), CNPq (Conselho Nacional de Desenvolvimento Cientifico e Tecnológico), FINEP (Financiadora de Estudos e Projetos), and Araucária Foundation. They are also thankful for the technical support of FUNPAR (Fundação da Universidade Federal do Paraná) and UFPR (Universidade Federal do Paraná).

Appendix A. Supplementary data

Supplementary data associated with this article can be found, in the online version, at http://dx.doi.org/10.1016/j.apcatb.2012.11.009.

References

[1] R.J. Batterham, Chemical Engineering Science 58 (2003) 2167.
[2] K. Narasimharao, A. Lee, K. Wilson, Journal of Biobased Materials and Bioenergy 1 (2007) 19.
[3] G.L.R. Vaccaro, C. Pohlmann, A.C. Lima, M.S. dos Santos, C.B. de Souza, D. Azevedo, Renewable and Sustainable Energy Reviews 14 (2010) 1263.
[4] C.S. Cordeiro, G.G.C. Arizaga, L.P. Ramos, F. Wypych, Catalysis Communications 9 (2008) 2140.
[5] L. Jin, Y. Zhanga, J.P. Dombrowskia, C.H. Chena, A. Pravatasc, L. Xua, C. Perkins, S.L. Suib, Applied Catalysis B: Environmental 103 (2011) 200–205.
[6] L.A.S. Nascimento, L.M.Z. Tito, R.S. Angélica, C.E.F. Costa, J.R. Zamian, G.N. Rocha Filho, Applied Catalysis B: Environmental 101 (2011) 495.
[7] M. Di Serio, M. Cozzolino, R. Tesser, P. Patrono, F. Pinzari, B. Bonelli, E. Santacesaria, Applied Catalysis A: General 320 (2007) 1.
[8] I. Jiménez-Morales, J. Santamaría-González, P. Maireles-Torres, A. Jiménez-López, Applied Catalysis B: Environmental 103 (2011) 91.
[9] Q. Shu, Q. Zhang, G. Xu, J. Wang, Food and Bioproducts Processing 87 (2009) 164.
[10] S.B. Umbarkar, T.V. Kotbagi, A.V. Biradar, R. Pasricha, J. Chanale, M.K. Dongare, A. Mamede, C. Lancelot, E. Payen, Journal of Molecular Catalysis A: Chemical 310 (2009) 150.
[11] S. Nakagaki, A. Bail, F.S. Nunes, V.C. dos Santos, V.H.R. de Souza, H. Vrubel, L.P. Ramos, Applied Catalysis A 351 (2008) 267.
[12] V.C. dos Santos, A. Bail, H.O. Okada, L.P. Ramos, K.J. Ciuffi, O.J. Lima, S. Nakagaki, Energy & Fuels 25 (2011) 2794.
[13] T. Jekewitz, N. Blickhan, S. Endres, A. Drochner, H. Vogel, Catalysis Communications 20 (2012) 25.
[14] S. Chavan, W. Maes, J. Wahlen, P. Jacobs, D. De Vos, W. Dehaen, Catalysis Communications 6 (2005) 241.
[15] G. Mitran, E. Mako, A. Redey, I.C. Marcu, Catalysis Letters 140 (2010) 32.
[16] T.M. Sankaranarayanana, A. Pandurangana, M. Banub, S. Sivasankerb, Applied Catalysis A: General 409–410 (2011) 239.

[17] C. Caro, K. Thirunavukkarasu, M. Anilkumar, N.R. Shiju, G. Rothenberga, Advanced Synthesis and Catalysis 354 (2012) 1327.
[18] L. Li, Y. Yoshinaga, T. Okuhara, Catalysis Letters 83 (2002) 231–234.
[19] X. Ma, J. Gong, S. Wang, N. Gao, D. Wang, X. Yang, F. He, Catalysis Communications 5 (2004) 101.
[20] A. El-Aziz, A. Said, M.M.M.A. El-Wahab, Journal of Chemical Technology and Biotechnology 81 (2006) 329.
[21] M.S. Saraiva, C.D. Nunes, T.G. Nunes, M.J. Calhorda, Journal of Molecular Catalysis A: Chemical 321 (2010) 92.
[22] M. Vasconcellos-Dias, C.D. Nunes, P.D. Vaza, P. Ferreira, P. Brandão, V. Felix, M.J. Calhorda, Journal of Catalysis 256 (2008) 301.
[23] N.U. Silva, T.G. Nunes, M.S. Saraiva, M.S. Shalamzaria, P.D. Vaza, O.C. Monteiro, C.D. Nunes, Applied Catalysis B: Environmental 113–114 (2012) 180.
[24] C. Marquesa, A.M. Sousa, C. Freire, I.C. Neves, A.M. Fonseca, C.J.R. Silva, Journal of Alloys and Compounds 360 (2003) 272.
[25] A.C. Coelho, S.S. Balula, S.M. Bruno, J.C. Alonso, N. Bion, P. Ferreira, M. Pillinger, A.A. Valente, J. Rocha, I.S. Gonçalves, Advanced Synthesis and Catalysis 352 (2010) 1759.
[26] K. Ambroziak, R. Mbeleck, Y. He, B. Saha, D.C. Sherrington, Industrial and Engineering Chemistry Research 48 (2009) 3293.
[27] L. Cao, M. Yang, G. Wang, Y. Wei, D. Sun, Journal of Polymer Science. Part A: Polymer Chemistry 48 (2010) 558.
[28] C.I. Fernandes, N.U. Silva, P.D. Vaza, T.G. Nunes, C.D. Nunes, Applied Catalysis A: General 384 (2010) 84.
[29] K.R. Jain, W.A. Herrmann, F.E. Kuhn, Coordination Chemistry Reviews 252 (2008) 556.
[30] K.A.D.F. Castro, M. Halma, G.S. Machado, G.P. Ricci, G.M. Ucoski, K.J. Ciuffi, S. Nakagaki, Journal of the Brazilian Chemical Society 21 (2010) 1329.
[31] A.T. Papacídero, L.A. Rocha, B.L. Caetano, E. Molina, H.C. Sacco, E.J. Nassar, Y. Martinelli, C. Mello, S. Nakagaki, K.J. Ciuffi, Colloids and Surfaces A 275 (2006) 27.
[32] C.J. Brinker, G.W. Scherer, Sol–gel Science: The Physics and Chemistry of Sol–gel Processing, 1st ed., Academic Press, San Diego, 1990.
[33] A.S. Alfaya, L.T. Kubota, Quimica Nova 25 (2002) 835.
[34] S. Brunauer, P.H. Emmett, E. Teller, Journal of the American Chemical Society 60 (1938) 309.
[35] E.P. Barrett, L.G. Joyner, P.P. Halenda, Journal of the American Chemical Society 73 (1951) 373.
[36] V.A. Murashov, A.V. Rozantsev, A.N. Klimenko, T.A. Zharinova, Russian Journal of Inorganic Chemistry 30 (1985) 2966.
[37] N.N. Greenwood, A. Earnshaw, Chemistry of the Elements, 2nd ed., Butterworth-Heinemann, Oxford, 1997.
[38] W.D. Callister Jr., Fundamentals of Materials Science and Engineering, 5th ed., John Wiley & Sons, Inc., New York, 2001.
[39] R.D. Gonzalez, T. Lopez, R. Gomez, Catalysis Today 35 (1997) 293.
[40] Z.M. Hanafi, M.A. Khilla, M.H. Askar, Thermochimica Acta 45 (1981) 221.
[41] S. Braun, L.G. Appel, V.L. Camorim, M. Schmal, Journal of Physical Chemistry B 104 (2000) 6584.
[42] E. McCarron III, J. Calabrese, Journal of Solid State Chemistry 91 (1991) 121.
[43] A. Hamoudi, A. Amoudi, L. Khouchaf, C. Depecker, B. Revel, L. Montagne, P. Cordier, Journal of Non-Crystalline Solids 354 (2008) 5074.
[44] JCPDS, International Centre for Diffraction Data, Card No. 36-0030 (1981).
[45] Y.V. Plyuto, I.V. Babich, I.V. Plyuto, A.D. Van Langeveld, J.A. Moulijn, Applied Surface Science 119 (1997) 11.
[46] S.O. Grim, L.J. Matienzo, Inorganic Chemistry 14 (1975) 1014.
[47] G. Rothenberg, Catalysis – Concepts and Green Applications, 1st ed., Wiley-VCH, Weinheim, 2008.
[48] G. Leofanti, M. Padovan, G. Tozzola, B. Venturelli, Catalysis Today 41 (1998) 207.
[49] C.B. Rodella, V.R. Mastelaro, Journal of Physics and Chemistry of Solids 64 (2003) 833.
[50] C. dos, S. Alfenas, G.P. Ricci, E.H. de Faria, M. Saltarelli, O.J. de Lima, Z.N. da Rocha, E.J. Nassar, P.S. Calefi, L.B. Montanari, C.H.G. Martins, K.J. Ciuffi, Journal of Molecular Catalysis A: Chemical 338 (2011) 65.
[51] J.R. Sohn, H.W. Kim, Y.I.I. Pae, Journal of Industrial and Engineering Chemistry 7 (2011) 160.
[52] D.M.A. Melo, W.S.C. Sousa, L.B. Zinner, M.A.F. Melo, H.E. Silva, A.G. Souza, Thermochimica Acta 328 (1999) 195.
[53] M.A. Melo, J.A.C. Ruiz, E.V. Sobrinho, M.A.F. Melo, A.E. Martinelli, L.B. Zinner, Journal of Solid State Chemistry 171 (2003) 217.
[54] K. Tanabe, T. Sumiyoshi, K. Shibata, T. Kiyoura, J. Kitagawa, Bulletin of the Chemical Society of Japan 47 (1974) 1064.
[55] R.L. Smith, G.S. Rohrer, Journal of Catalysis 184 (1999) 49.
[56] R.J. Madon, M. Boudart, Industrial and Engineering Chemistry Fundamentals 21 (1982) 438.
[57] R.M. Korus, E.J. Novak, Chemical Engineering Science 22 (1967) 470.
[58] I. Balint, A. Miyazaki, K. Aika, Reaction Kinetics and Catalysis Letters 85 (2005) 189.
[59] J. Bernholc, J.A. Horsley, L.L. Murrel, L.G. Sherman, S. Soled, Journal of Physical Chemistry 91 (1987) 1526.
[60] D.M. Alonso, M.L. Granados, R. Mariscal, A. Douhal, Journal of Catalysis 262 (2009) 18.
[61] D. Rattanaphra, A.P. Harvey, A. Thanapimmetha, P. Srinophakun, Renewable Energy 36 (2011) 2676.
[62] I. Zhang, B. Sheng, Z. Xin, Q. Liu, S. Sun, Bioresource Technology 101 (2010) 8144.
[63] M. Berrios, J. Siles, M.A. Martín, A. Martín, Fuel 86 (2007) 2383.
[64] D.J. Vujicic, D.D. Comic, A. Zarubica, R. Micic, G. Boskovic, Fuel 89 (2010) 2054.